

RSC Advances



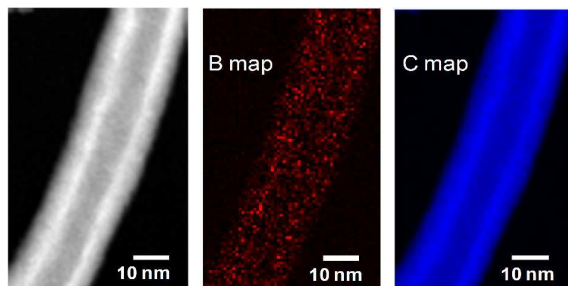
This is an *Accepted Manuscript*, which has been through the Royal Society of Chemistry peer review process and has been accepted for publication.

Accepted Manuscripts are published online shortly after acceptance, before technical editing, formatting and proof reading. Using this free service, authors can make their results available to the community, in citable form, before we publish the edited article. This *Accepted Manuscript* will be replaced by the edited, formatted and paginated article as soon as this is available.

You can find more information about *Accepted Manuscripts* in the [Information for Authors](#).

Please note that technical editing may introduce minor changes to the text and/or graphics, which may alter content. The journal's standard [Terms & Conditions](#) and the [Ethical guidelines](#) still apply. In no event shall the Royal Society of Chemistry be held responsible for any errors or omissions in this *Accepted Manuscript* or any consequences arising from the use of any information it contains.

Table of Contents



An atmospheric-pressure substitution reaction to produce B-doped CNTs with controllable and uniform B distributions has been demonstrated.

Controllable boron doping carbon nanotubes with tunable dopant functionalities: an effective strategy toward carbon materials with enhanced electrical properties

Wei-Hung Chiang^{1*}, Guan-Lin Chen¹, Cheng-Yu Hsieh², and Shen-Chuan Lo²

¹Department of Chemical Engineering, National Taiwan University of Science and Technology, Taipei 10607, Taiwan

²Material and Chemical Research Laboratories, Industrial Technology Research Institute, Hsinchu, 30013, Taiwan.

Abstract

We present a two-step postgrowth substitution reaction route to produce boron-doped carbon nanotubes (BCNTs) with controllable B dopant concentration and uniform B atom distribution under atmospheric pressure. The unique two-step postgrowth substitution reaction route composed a simple wet-chemistry-assisted pretreatment and an atmospheric-pressure carbothermic reaction. Extensive materials characterizations confirmed that BCNTs with uniform B dopant distribution and controllable B atomic concentrations from 0.40 to 3.92 atomic percent (atom %) can be produced by controlling the reaction time and temperature under atmospheric pressure in the developed method. The film-based electrical sheet resistance measurement indicates that the averaged electrical sheet resistances of the as-fabricated CNT-based films can be improved from 1520 ± 197.56 to $43.67 \pm 12.63 \Omega \text{ square}^{-1}$ with 2.09 atom % B concentration in the doped CNTs. High-resolution X-ray photoelectron spectroscopy (HRXPS) characterization suggests that the B-C-O bonding types and concentrations in the as-produced BCNTs may play an important role on the nanotube electrical properties. Our research provides a methodology to tailor the materials properties of carbon-based materials.

Keywords: carbon nanotube; doping; boron; atmospheric pressure; synthesis

*Corresponding author: E-mail address: whchiang@mail.ntust.edu.tw (W.-H. Chiang)

Introduction

Heteroatom doping has been shown as an effective approach to tailor the physical and chemical properties of carbon nanomaterials including carbon nanotubes (CNTs) and graphene¹⁻⁵. Among the doping elements, electron-deficient boron (B) is considered to be a promising candidate since it has only three valence electrons, making it possible to modify the chemical inert sp² carbon structure by activating the abundant free-flowing π electrons. In addition, the introduction of B also increases the number of hole-type charge carriers, which enhance the electrical conductivity of carbon materials obviously. Recent theoretical and experimental studies have suggested that boron-doped CNTs (BCNTs) as the materials with exceptional properties for applications including nanoelectronics and optoelectronics⁶⁻⁹, energy storage and conversion¹⁰⁻¹², catalysis^{13, 14}, and electrochemical sensing¹⁵,¹⁶. Nevertheless, there are few reports investigating the effect of the boron dopant concentrations in CNTs on their physical and chemical properties such as electrical conductivity. The difficulty is because of the lacking of effective methods to precisely control the boron dopant concentrations on the carbon surface.¹⁷⁻¹⁹ Consequently the development of a controllable and scalable synthesis of BCNTs will lead to important advances on both scientific studies and innovation applications.

In general, there are two approaches to produce BCNTs including the direct growth by means of chemical vapor deposition (CVD)²⁰⁻²², arc discharge²³, and laser ablation²⁴, and the postgrowth substitution reaction²⁵⁻³⁰. While the direct growth approach is capable to produce BCNTs with high crystallinity, the excess B in the feedstock are usually existed in the form of by-products such as boron carbide (B₄C), boron nitrate (BN), and boron particles which could affect the final properties of the as-produced BCNTs²³. Moreover, the process usually involves complicated synthesis system and requires a high-vacuum condition, making it difficult to enable industrial-scale and low-cost production^{20, 22}. On the other hand, the postgrowth substitution reaction usually undergoes a carbothermal reaction with the vapor of B-contained precursor and the presynthesized CNTs as a starting materials at elevated temperature (normally 1000-1700 °C) under a chemical inert gas

(normally nitrogen or argon) atmosphere²⁵⁻²⁹. Under suitable reaction conditions, B atoms are incorporated into the honeycomb tube-shell lattice of the CNTs, thereby resulting in the formation of the BCNTs. While recent works have demonstrated the successful synthesis of BCNTs in large quantities using postgrowth reaction approach, it was found to be less effective to produce BCNTs with controllable dopant concentrations and distribution on CNT surface and therefore limits their applications due to the uncontrolled materials properties²⁵⁻²⁹. The difficulty lies in the bundling phenomena of the starting CNTs. As a result of the extraordinary interaction between neighboring nanotubes due to van der Waals interaction, CNTs have a strong tendency to spontaneously form densely bundled ropes in their native state. When the bundled CNTs are subjected to the postgrowth substitution reaction, only the small fraction of CNTs localized at the outermost fractions of the bundles are chemically accessible to the gaseous B-contained reactants. Recently, a wet-chemistry-assisted method has been shown an effective method to overcome the CNT aggregation problem with the assistance of ionic liquids and to produce heteroatom-doped CNTs under vacuum condition³⁰. However, It is still needed to develop a scalable and controllable method to produce BCNTs with controlled B concentration and distribution on CNT surface under atmospheric pressure.

Here we report a stepwise postgrowth substitution reaction route to produce BCNTs with controllable B dopant concentrations and uniform B distributions under atmospheric pressure (Fig. 1). The unique stepwise postgrowth substitution reaction route composed a simple wet-chemistry-assisted pretreatment and an atmospheric-pressure carbothermic reaction. Pristine multi-walled CNTs (MWCNTs) synthesized using a scalable water-assisted chemical vapor deposition (CVD) were used as the starting materials³¹. The first and key step of this approach was the wet-chemistry-assisted pretreatment by dispersing the starting MWCNTs in a sodium dodecyl sulfate (SDS) aqueous solution. Previously the low-cost SDS has been reported as an effective surfactant to disperse CNTs in aqueous solution³². Boron oxide (B_2O_3) powder used as the B precursor was then added into the CNT/SDS dispersion at 80 °C. B_2O_3 is very soluble in hot water, forming boric acid and a variety of ionic

molecules which can mixed well with the dispersed CNTs³³. Last, the CNTs and the boron precursors were filtered, collected and dried into a mixed powder. We used this approach with the aim of homogeneously distributing the B precursors over the CNT surfaces. The BCNTs were produced by heating the as-prepared mixed powder of B-precursor-wrapped CNTs under Ar atmosphere from 1000 to 1200 °C for 4 and 8 hours (h) at atmospheric pressure. We find that a yield of 5.24 g/h in a single batch process (after purification) can be achieved using our experimental setup. Extensive scanning electron microscopy (SEM), high-resolution transmission electron microscope (HRTEM), X-ray photoelectron spectroscopy (XPS), micro Raman, and X-ray diffraction (XRD) characterizations confirmed that compositionally-tuned BCNTs can be produced using the developed method. Detailed atomic-scale HRTEM electron energy loss spectroscopy (HRTEM-EELS) characterization significantly indicated that the B dopants were uniformly distributed on the surfaces of as-produced BCNTs, and secondary phase of B₄C and B particles were not existed in the as-produced BCNTs. Systematic HRXPS characterization indicated the B dopant concentrations of the as-produced BCNTs were controllable from 0.40 to 3.92 at % by controlling the reaction conditions (time and temperature), which is significantly higher than that of BCNT produced without wet-chemistry-assisted pretreatment under the same reaction conditions. The film-based electrical sheet resistance measurement using a four-point probe suggested that the electrical properties of the as-produced BCNTs were improved after B doping. It is found that the averaged sheet resistivity decreases largely from $1520 \pm 197.56 \text{ } \Omega \text{ square}^{-1}$ to $43.67 \pm 12.63 \text{ } \Omega \text{ square}^{-1}$ when incorporating a small amount of B atoms (2.09 at%) in the as-produced BCNTs. The high-resolution XPS (HRXPS) characterization reveals that the B-C bonding type (BC₃, BC₂O, and BCO₂) of the as-produced BCNTs were very sensitive to the reaction conditions and suggests that the B-C-O bonding types and concentrations in the as-produced BCNTs may play an important role on the nanotube electrical property. It is noteworthy from a practical point of view that the developed atmospheric-pressure synthesis method is amenable to industrial-scale production since it avoids the need for a vacuum system and also simultaneously solved the basic obstacles of simple sample preparation, easy process operation, and scalable possibility.

Experimental section

Materials and chemicals

Deionized water (DI-water) with a resistivity $\geq 18.2 \text{ M}\Omega\text{-cm}$ was produced by Purelab Maxima (ELGA, UK). Boron trioxide powder (B_2O_3 , ACS reagent, $\geq 99\%$) and sodium dodecyl sulfate (SDS, ACS reagent, $\geq 99\%$) were purchased from Alfa Aesar (Lancashire, United Kingdom). The chemicals were used as received without further purification.

BCNT synthesis

The starting CNTs used in the present study were multi-walled CNTs (MWCNTs) synthesized using a catalytic chemical vapor deposition (CVD). Details of the MWCNT growth process were similar to that previously described and detailed in the supporting information^{31, 34}. The as-synthesized MWCNTs processes high crystallinity and uniform length, diameter, and wall-number distributions, making them good starting materials to produce BCNTs. To produce BCNTs with controllable B dopant concentrations and uniform B distributions, we have developed a simple postgrowth substitution reaction route composed with a wet-chemistry-assisted pretreatment and atmospheric-pressure carbonthermal reaction (Figure 1). The starting CNTs were dissolved in a 1 wt% SDS aqueous solution to form a well dispersion (typical CNT concentration: 1 wt%). We then dissolved B_2O_3 powder in the CNT/SDS dispersion at $80 \text{ }^\circ\text{C}$, and the solution stirred using a magnetic-stirred bar under 500 rpm until the solution became a slurry-like paste. The paste was collected and then dried into a mixed powder in an oven with $60 \text{ }^\circ\text{C}$. The mixed CNT and boron precursor was placed in an alumina boat and then introduced into an alumina tube reactor (3 inch outside diameter) filled with Ar gas at atmospheric pressure. The system was first heated for 2 h at $150 \text{ }^\circ\text{C}$ to remove all the moisture with the Ar gas flowing at a rate of 300 sccm. Subsequently the temperature was raised to high temperatures from 1000 and $1200 \text{ }^\circ\text{C}$ for 4 to 8 h. Detailed reaction conditions are summarized in Table S1. When the reaction was complete, the material was retrieved from the boat and the possible excess of physisorbed boron/boron oxide was removed by washing

with hot water (80 °C) several times until the pH value of the filtrate was close to 7. The washed materials were filtered by Polytetrafluoroethylene (PTFE) membrane with a pore size of 1 µm. The material on top of the membrane was collected and dried into a mixed powder in an oven with 60 °C.

Characterizations

Ex situ characterization of the starting CNTs and as-produced BCNTs were performed by SEM, TEM, EELS, XPS, microRaman, and XRD. XPS (VG ESCALAB 250, Thermo Fisher Scientific, UK) was performed with a monochromatic Al K α X-ray radiation (10kV, 10 mA) to quantify the amount of boron doped into the MWCNT. The source power was set at 72 W, and pass energies of 200 eV for survey scans and 50 eV for high-resolution scans were used. Spectra were normalized by the C-1s intensity and averaged from 5 different samples from the same batch. Cold-field emission Cs-corrected TEM (JEOL ARM-200F, Japan) with 200 kV accelerating voltage was used to observe the morphologies of CNTs. Carbon-coated copper grids (400 mesh) were used in the TEM sample preparation. EELS observations were conducted on a JEOL ARM-200F TEM instrument to characterize the K-edge absorption of carbon and boron. The energy resolution measured by the full width at half maximum of a zero-loss peak was about 0.4 eV through a cold field emission gun and the probe size is about 1.5-2 Å. Additional assessment of the morphology of as-produced BCNTs was attained by micro-Raman spectroscopy. Raman scattering studies were performed at room temperature with a JASCO 5100 spectrometer ($\lambda = 533$ nm). Spectra were normalized by the G-band intensity and averaged from 10 random positions on each sample. XRD characterization was performed to determine the crystalline structure of the as-produced BCNTs with a Scintag X-1 advanced X-ray diffractometer using monochromated Cu K α radiation ($\lambda = 0.1542$ nm). All the experiments were conducted at room temperature. Direct current (DC) electrical conductivity was measured using the 4-point probe method (Loresta GP Model MCP-T610, Mitsubishi Chemical). Sheet resistances were averaged from 10 random positions on each film. Thin films of the pristine and as-produced BCNTs were prepared with the following procedures. 5 mg of pristine CNTs and

the as-produced BCNTs were dissolved with 10 mL of DI water and the mixture was homogenized at 20,000 rpm for 10 minutes (Ultra Turrax T25, IKA). The dispersed materials were filtered by Polyvinylidene fluoride (PVDF) membrane with a pore size of 1 μm . The materials on top of the membrane were collected and dried into a film in an oven with 60 $^{\circ}\text{C}$ for 24 h.

Results and discussion

Representative SEM and TEM images of starting CNTs [Fig. 2(a)-(c)] and the as-produced BCNTs (sample B3 in Table S1) were shown in Fig. 2, indicating that the as-produced BCNTs remained the tubular structure after the high temperature reaction [Fig. 2(d)-(f)]. The HRTEM image [Fig. 2(f)] indicated that the as-produced BCNTs have straight and smooth tube-shell structures with a diameter distribution similar to that of the starting MWCNTs before the substitution reaction. Moreover, the detailed HRTEM investigation reveals the absence of byproducts including amorphous carbon coating or B_4C particles on the nanotube walls, suggesting that it is possible to avoid the formation of byproducts during the reaction of BCNTs using the developed method.

The elemental compositions of the as-produced BCNTs were further carefully examined using EELS. We were careful to focus the TEM beam on only clean bundles of as-produced BCNTs to minimize the contributions from byproducts or B-doped amorphous carbon nanostructures. Representative EELS spectrum of the as-produced BCNTs (sample B3 in Table S1) was shown in Fig. 3(a). The EELS spectrum clearly exhibits the definite core-loss K-edges of showing both the C and B characteristic K-shell peaks. The intense C K-edge shows maximum peaks at 284 ($1s \rightarrow \pi^*$ transition) and 291 eV ($1s \rightarrow \sigma^*$ transition), and the B K-edge presents maximum peaks at 191 eV ($1s \rightarrow \pi^*$ transition) [Fig. 3(b)], indicating the sp^2 -bonded B-C hybridization to confirm that we achieved the true substitutional incorporation of B dopants into the nanotube lattice^{29,30,35}. It is important to note that pure B does not present the $1s \rightarrow \pi^*$ sharp peak at 191 eV characteristic of the sp^2 hybridization; instead only a broad peak centered around 200 eV should be observed^{36,37}. Moreover we did not observe the EELS peak at 194 eV corresponding to B_2O_3 impurities²⁸ and any sulfate-related peaks.

The EELS result clearly indicated the absence of B clusters, B₄C or B₂O₃ impurities as well as the SDS-related moieties on the nanotube walls of as-produced BCNTs. Importantly nearly identical EELS spectra were also obtained for numerous EELS runs at different probe positions on the same batch of sample, indicating that the as-produced BCNTs have fairly homogeneous elemental compositions. Quantification of the EELS result gave a averaged dopant concentrations of 1.5 atom percentage (atom %) for B in sample B3. We therefore conclude that the majority of the boron in the as-produced BCNTs has been incorporated into the sp² nanotube carbon network. Detailed EELS elemental mapping was performed to study the B dopant distribution on the surface of as-produced BCNTs³⁸. Fig. 3(c) shows the high-angle annular dark-field imaging (HAADF) image of an individual as-produced BCNT, and the corresponding B and C mappings using scanning TEM (STEM) EELS were shown in Fig. 3(d) and (e), respectively. The B mapping clearly illustrates a homogeneous distribution of B atoms incorporated into the sp²-bonded atomic structure of nanotubes. According to the above analysis, it is evident that we have successfully produced BCNTs with uniform B dopant distribution on the nanotube surface using the developed postgrowth substitution reaction.

To show our method is capable to control the B dopant concentrations in the as-produced BCNTs, different samples were prepared with the same starting materials treated by the developed pretreatment (Fig. 1) but under different reaction temperatures and times (sample B1-B6 in Table S1). We have also performed the reactions of BCNTs from starting materials without the wet-chemistry-assisted pretreatment as a comparison (sample A1-A3 in Table S1). XPS was employed to identify the element composition of starting CNTs and as-produced BCNTs. Representative XPS spectra of starting CNTs (sample P), sample A3, B3, and B6 (reaction conditions listed in Table S1) are shown in Fig. 4(a) while the XPS spectra of other samples are shown in Figure S1. Spectra were normalized by the C1s (284.6 eV) intensity and averaged from 10 random positions on each sample. The peaks around 190.8, 284.6, and 534.6 eV respectively assigned to B1s, C1s, and O1s were observed for all as-produced BCNTs while only peaks for C1s and O1s obtained for the starting CNTs^{12, 22, 30}. This result supported

that B atoms were existed in the structure of as-produced BCNTs and agreed with the EELS results (Figure 2) and previous reports^{39, 40}. Oxygen peaks could be due to the oxidation of as-produced BCNTs¹². The enlarged B1s region (184–196 eV) of spectra were shown in Fig. 4(b) and Fig. S2(b). We carefully estimate the B dopant concentrations in each sample using XPS elemental quantification^{12, 40} and found that the B dopant concentrations in the as-produced BCNTs were very sensitive to the pretreatment and reaction conditions. Fig. 4(c) shows the quantified B dopant concentrations in the as-prepared BCNTs as the function of reaction temperature. It is noted that the B dopant concentrations in the as-produced BCNTs prepared with the developed pretreatment and 4 h reaction time were varying from 0.4 to 2.09 at% under different temperatures while those in the as-produced BCNTs prepared without the developed pretreatment and 4 h reaction time were only from 0.08 to 0.04 at%, showing our pretreatment processes the ability to overcome the CNT aggregation problem and to produce BCNTs with higher B dopant concentrations. Significantly, we found that the B dopant concentrations in the as-produced BCNTs prepared with the developed pretreatment can further increased up to 3.92 at% by increasing the process time to 8 h under 1200 °C, indicating that our method is effective on the production of BCNTs with controllable B dopant concentrations by simply controlling the reaction temperature and time under atmospheric pressure. From our experiments performed with temperatures between 900 to 1200 °C and the XPS characterization, it is found that BCNTs could not be produced with the reaction temperature below 1000 °C. Early study of temperature programmed desorption (TPD) and XPS have been used to study the oxidation of graphitic carbon by B₂O₃, and the result suggests that B₂O₃ may be reduced by carbon at temperatures above 700 °C and the reaction was very sensitive to the temperature⁴¹. Previous report discusses a sequential reaction steps in the BCNT synthesis using a postgrowth substitution reaction route²⁹. In general B₂O₃ was melted and then vaporized with increasing temperature in the tubular furnace, and some carbon atoms in the nanotube walls were oxidized and form CO gas. The vacancies left by these carbon atoms could eventually be filled with the remaining boron atoms. It is also suggested that the original defects in the graphene framework of CNTs could provide active sites for boron doping.

Consequently, BCNTs can be synthesized through thermal annealing CNTs in the presence of B_2O_3 , where boron atoms coming from B_2O_3 vapor replace carbon atoms within graphene structures of CNTs at high temperature. According to the previous reports and our experimental results, we suggest that BCNTs could be produced by thermal annealing CNTs in the presence of B_2O_3 with the temperature between 1000 to 1200 °C under atmospheric pressure, and 1000 °C was the onset temperature for B doping into nanotubes in our experiments. Based on the XPS result, we found that the pretreatment, temperature, and time of the substitution reaction were crucial factors that sensitively affect the B doping process of CNTs in our present study^{22, 27}. The analysis result is summarized in Table S1.

Complementary evidence for the substitutional incorporation of B atoms into the tube-shell lattice of the CNTs was also provided by HRXPS characterization (Fig. 5 and Fig. S2). For the high resolution C1s spectrum of as-produced BCNTs (sample A3, B3, and B6) [Fig. 5(a)-(c)], the new and relatively weak C-O-B (289.4eV) and C-B (283.9 eV) peaks related to B-doped structure can be seen in the sample B3 and B6 while no clear C-O-B (289.4eV) and C-B (283.9 eV) peaks were found in the sample A3, indicating the successful doping of boron atoms can be achieved in our developed method^{42, 43}. The detailed HRXPS spectra of as-produced BCNTs (sample A3, B3, and B6) in a range of 184~200 eV reveal the existence of B species [Fig. 5(d)-(f)]. The Gaussian deconvolution analysis indicated that the spectrum can be divided into five peaks with various intensities, which are centered at 187, 187.8, 189.9, 190.9, and 191.8 eV, corresponding to B-B, B_4C , BC_3 , BC_2O , and BCO_2 chemical configurations, respectively^{22, 39, 40}. The B doping chemical configurations are depicted in Fig. 5(g). It is noticed that byproducts including boron cluster, and B_4C were found in the as-produced samples without pretreatment process (A1-A3), confirming that the bundled behavior of CNTs created difficulty to produce BCNTs with high purity. In the contrast, all the as-produced samples treated with pretreatment process (B1-B6) show no secondary phase of boron-related byproducts [Fig. 5(d)-(f) and Fig. S3], which is in consistent with the HRTEM-EELS characterization (Fig. 3). It is noticed that the

BC₃ doping concentrations in the as-produced BCNTs were increased with the increased reaction temperature and time while the BC₂O and BCO₂ doping concentrations were decreased with the increased reaction temperature and time (Table S2). Previous work suggests that oxygen-containing doping bonds have low thermal stabilities at high temperatures and their concentrations were decreased with the increased reaction temperature and time⁴⁴.

Further structural information about as-produced BCNTs can be obtained from micro Raman spectra measurements. Fig. 6(a) shows the representative Raman spectra of pristine CNTs and as-produced BCNTs. Two bands are present around 1340 cm⁻¹ and 1590 cm⁻¹ which are respectively assigned to the presence of disorders in carbon systems (D band) and to the in-plane vibration of the C–C bond (G band)⁴⁵. Generally the value of the intensity ratio of D band to G band (I_D/I_G) is used to estimate the degree of disorder and defects of carbon materials⁴⁵. The I_D/I_G versus the B dopant concentrations in the as-synthesized BCNTs is plotted in Fig. 6(b). It is found that the I_D/I_G was increased with the increasing B dopant concentrations in the as-produced BCNTs. These Raman features can be rationalized as a consequence of the substitutional doping of CNTs with B atoms,^{13,45,46}. The G-band frequency can be used to distinguish between metallic and semiconducting CNTs and to probe the charge transfer arising from heteroatoms doped in CNTs⁴⁵. Fig. 6(c) shows that the G⁻ band feature for the as-produced BCNTs consists of two main components, one peaked at 1610 cm⁻¹ (G⁺) and the other peaked at about 1580 cm⁻¹ (G⁻). The corresponding G⁺ frequency (ω_G^+) and G⁻ frequency (ω_G^-) frequencies of the as-produced BCNTs are shown in the Fig. 6(d). Taking the pristine CNTs as the reference, it is found that a up-shifts in ω_G^+ was found in all the as-produced BCNT samples, suggesting that B dopants play as the acceptors in the graphene network of CNTs^{45,47}. In contrast, we noticed a down-shift of ω_G^- was found in all the as-produced BCNT samples, implying the as-produced BCNTs became more metallic than the pristine CNTs^{45,48}.

The crystalline structure of the pristine CNTs and as-produced BCNTs was further characterized by XRD. Fig. 7(a) represents the XRD patterns of pristine CNTs and as-produced BCNTs.

Broadening of diffraction peaks was observed for pristine CNT and as-produced BCNT thin films, indicating that samples were composed of nanostructures⁴⁹. The diffraction peak at 25.90 of 2θ value is ascribed to the (002) crystalline hexagonal planes of graphite, and the corresponding lattice spacings calculated from Bragg's law are 0.344 nm. This result is in good agreement with previous report⁴⁹. The XRD patterns of as-produced BCNTs can be indexed to the (002) Bragg peak with shifting to higher angles, which is attributed to the substitution of boron in the carbon network^{50, 51}. To reveal the relationship between the B dopant concentrations and the crystalline structures of the as-produced BCNTs, 2θ values of (002) Bragg peak in the XRD patterns of as-produced BCNTs were extracted to perform quantitative calculation using Bragg's law. Fig. 7(b) and (c) present the plots of $\Delta 2\theta$, the (002) Bragg peaks position difference between the as-produced BCNTs and pristine CNTs, and calculated interlayer spacing of (002) plane as the functions of B dopant concentrations in the as-produced BCNTs, respectively. Linear fittings are also shown for comparison. It is noted that as the B content in the as-produced BCNTs was increased from 0.4 to 3.92 atom %, the $\Delta 2\theta$ and calculated interlayer spacing of (002) plane were increased and decreased linearly, respectively. The decreasing corresponding lattice spacings (002) plane of the as-produced BCNTs suggests the stress formation of the nanotube as a result of B atom substitution, which is consistent with previous reports for bulk bornated carbons and B-substituted carbons with B atomic concentration below 10 atom %^{51, 52} as well as BCNTs and B-doped graphene with low B atomic concentration^{50, 53}. Overall, the micro Raman and XRD characterizations suggest that the atomic structure of starting CNTs were changed after B substitution doping into the carbon network of nanotubes, which might affect the electrical property of starting CNTs.

To study the effect of the B doping on the electrical property of the as-produced BCNTs, the sheet resistances of the films fabricated by the pristine CNTs and the as-synthesized BCNTs with various B dopant concentrations were evaluated using a four-point-probe measurement. The film fabrication and the amount of solid materials in each film were carefully controlled to fix the film

thickness. The sheet resistances were averaged from 10 random positions on each sample. Fig. 8 (a) shows the sheet resistances of the films of pristine CNTs and the as-synthesized BCNTs with varying B dopant concentrations. It is significantly found that the averaged sheet resistance decreases largely from 1520 ± 197.56 to $87.56 \pm 16.26 \Omega \text{ square}^{-1}$ when incorporating a small amount of B atoms (0.4 at%; sample B1) in CNTs. The average sheet resistance was further reduced with the increased B dopant concentration of as-produced BCNTs, and the lowest value ($43.67 \pm 12.63 \Omega \text{ square}^{-1}$) was obtained with 2.09 atom% of B dopant concentration in the as-produced BCNTs (sample B3), indicating the best electrical conductivity for this case [inset of Fig. 8(a)]. It is also noted the smaller standard deviations of the sheet resistances measured in the BCNT samples than that of the pristine CNTs. The result suggested that as-produced BCNTs process improved electrical property due to the uniformly B substitutional doping by the developed process [Fig. 3 (d)].

Previous reports propose that an increase in free carrier concentration due to the B-doping could induce a decrease of the sheet resistance in the CNT-based films^{3,35}. However, higher B dopant concentration (>2.09 atom%; sample B4-B6) causes increased sheet resistances for the BCNTs. The defect creation for pristine CNTs with higher B dopant concentrations as shown in the Raman analysis [Fig. 6(b)] were likely to increase the number of scattering centers, thus reducing the electrical conductivity. In addition, the variation in the amount of various B-C bonding configurations in the as-produced BCNTs is critical and may influence the electrical conductivity of the as-produced BCNTs. To further understand the effect of the B-C bonding configurations on the electrical property of the as-produced BCNTs, the distributions of B-C bonding configurations in the as-produced BCNTs from the HRXPS result (Fig. 5 and Fig. S2) were carefully examined, and the statistic result is shown in Fig. 8(b). It was found that the atomic percentage of the BC₃ bonding was increased for the BCNTs with increasing B dopant concentrations from 0.4 to 2.09 atom % (sample B1 to B3) and reaches 0.66 atom % of BC₃ doping type for the BCNTs (sample B3). Previous work suggests that the graphite-like BC₃ dopant specie can improve the electrical conductivity of B-doped carbon materials because the valence

band structure and the density of states near the Fermi level of the carbon materials can be changed^{3,54}. Subsequently the BC₃ dopant atomic percentage was decreased to 0.16 atom % (sample B4) and was increased to 0.53 and 1.25 atom % with increasing B atomic dopant concentrations in the as-produced BCNTs (sample B5 and B6), suggesting that the concentration of BC₃ doping type in the as-produced BCNTs was very sensitive to the reaction conditions (e.g. temperature and time). While BCNTs with 3.92 atom % of B (sample B6) exhibits the highest atomic percentage of BC₃ (1.48 atom %), high percentage of boron dopants in oxidized states including BC₂O and BCO₂ and defect level suggested from Raman result may lower its electronic conductivity due to electrons trapped by these active functional groups^{55,56}. This finding may be the origin why we observed the BCNTs with 2.09 atom % B-doping gave the lowest averaged sheet resistivity ($43.67 \pm 12.63 \Omega \text{ square}^{-1}$). Our study suggests that the controllable synthesis of BCNTs with tunable BC₃ to B-C-O percentage will be helpful to further improve the electrical conductivity of carbon-based materials.

Conclusions

In summary, we have demonstrated a two-step postgrowth substitution reaction route to produce BCNTs with controllable B dopant concentrations and uniform B distributions under atmospheric pressure. The unique two-step postgrowth substitution reaction route composed a simple wet-chemistry-assisted pretreatment and an atmospheric-pressure carbothermic reaction. Extensive materials characterizations confirmed that BCNTs with uniform B dopant distribution and controllable B atomic concentration from 0.40 to 3.92 atom % can be produced by simply controlling the reaction conditions (time and temperature) under atmospheric pressure using the developed method. The film-based electrical sheet resistance measurement indicates that the electrical property of the as-produced BCNTs can be improved by B substitutional doping, suggesting B-C-O bonding types and concentrations in the BCNTs may play an important role on the electrical property of carbon nanomaterials. Our study provide a methodology to systematic study the physical and chemical properties of heteroatom-doped carbon nanomaterials.

Acknowledgments

This work was supported by the Ministry of Science and Technology of Taiwan (MOST Grant no. MOST 103-2221-E-011-150-MY2 and MOST 104-2923-E-011-001-MY3), National Taiwan University of Science and Technology (NTUST) and Industrial Technology Research Institute (ITRI).

Associated content

Supporting Information Available: Details of CNT synthesis and B doping reaction conditions. XPS spectra and HRXPS B1s core-level spectra of as-produced BCNTs. This material is available free of charge via the Internet.

References

1. R. H. Baughman, A. A. Zakhidov and W. A. de Heer, *Science*, 2002, **297**, 787-792.
2. M. F. L. De Volder, S. H. Tawfick, R. H. Baughman and A. J. Hart, *Science*, 2013, **339**, 535-539.
3. P. Ayala, R. Arenal, A. Loiseau, A. Rubio and T. Pichler, *Rev. Mod. Phys.*, 2010, **82**, 1843-1885.
4. M. Terrones, A. Jorio, M. Endo, A. M. Rao, Y. A. Kim, T. Hayashi, H. Terrones, J. C. Charlier, G. Dresselhaus and M. S. Dresselhaus, *Mater. Today*, 2004, **7**, 30-45.
5. M. H. Yeh, Y. S. Li, G. L. Chen, L. Y. Lin, T. J. Li, H. M. Chuang, C. Y. Hsieh, S. C. Lo, W. H. Chiang and K. C. Hoa, *Electrochim. Acta.*, 2015, **172**, 52-60.
6. B. Q. Wei, R. Spolenak, P. Kohler-Redlich, M. Ruhle and E. Arzt, *Appl. Phys. Lett.*, 1999, **74**, 3149-3151.
7. G. G. Fuentes, E. Borowiak-Palen, M. Knupfer, T. Pichler, J. Fink, L. Wirtz and A. Rubio, *Phys. Rev. B*, 2004, **69**, 245403.
8. P. Ayala, W. Plank, A. Gruneis, E. I. Kauppinen, M. H. Rummeli, H. Kuzmany and T. Pichler, *J. Mater. Chem.*, 2008, **18**, 5676-5681.
9. B. Anand, R. Podila, P. Ayala, L. Oliveira, R. Philip, S. S. S. Sai, A. A. Zakhidov and A. M. Rao, *Nanoscale*, 2013, **5**, 7271-7276.
10. J. P. Paraknowitsch and A. Thomas, *Energy Environ. Sci.*, 2013, **6**, 2839-2855.
11. I. Mukhopadhyay, N. Hoshino, S. Kawasaki, F. Okino, W. K. Hsu and H. Touhara, *J. Electrochem. Soc.*, 2002, **149**, A39-A44.
12. V. Saini, Z. R. Li, S. Bourdo, V. P. Kunets, S. Trigwell, A. Couraud, J. Rioux, C. Boyer, V. Nteziyaremye, E. Dervishi, A. R. Biris, G. J. Salamo, T. Viswanathan and A. S. Biris, *J. Appl. Phys.*, 2011, **109**, 014321.
13. L. J. Yang, S. J. Jiang, Y. Zhao, L. Zhu, S. Chen, X. Z. Wang, Q. Wu, J. Ma, Y. W. Ma and Z. Hu, *Angew. Chem. Int. Ed.*, 2011, **50**, 7132-7135.
14. Y. H. Cheng, Y. Y. Tian, X. Z. Fan, J. G. Liu and C. W. Yan, *Electrochim. Acta.*, 2014, **143**, 291-296.

15. C. Y. Deng, J. H. Chen, X. L. Chen, C. H. Mao, L. H. Nie and S. Z. Yao, *Biosens. Bioelectron.*, 2008, **23**, 1272-1277.
16. C. Y. Deng, J. H. Chen, X. L. Chen, M. D. Wang, Z. Nie and S. Z. Yao, *Electrochim. Acta.*, 2009, **54**, 3298-3302.
17. W. Han, Y. Bando, K. Kurashima and T. Sato, *Chem. Phys. Lett.s*, 1999, **299**, 368-373.
18. E. Borowiak-Palen, T. Pichler, A. Graff, R. J. Kalenczuk, M. Knupfer and J. Fink, *Carbon*, 2004, **42**, 1123-1126.
19. Y. A. Kim, S. Aoki, K. Fujisawa, Y. I. Ko, K. S. Yang, C. M. Yang, Y. C. Jung, T. Hayashi, M. Endo, M. Terrones and M. S. Dresselhaus, *J. Phys. Chem. C*, 2014, **118**, 4454-4459.
20. P. Ayala, M. H. Rummeli, T. Gemming, E. Kauppinen, H. Kuzmany and T. Pichler, *Phys. Status Solidi B*, 2008, **245**, 1935-1938.
21. B. C. Satishkumar, A. Govindaraj, K. R. Harikumar, J. P. Zhang, A. K. Cheetham and C. N. R. Rao, *Chem. Phys. Lett.*, 1999, **300**, 473-477.
22. F. H. Monteiro, D. G. Larrude, M. E. H. M. da Costa, L. A. Terrazos, R. B. Capaz and F. L. Freire, *J. Phys. Chem. C*, 2012, **116**, 3281-3285.
23. O. Stephan, P. M. Ajayan, C. Colliex, P. Redlich, J. M. Lambert, P. Bernier and P. Lefin, *Science*, 1994, **266**, 1683-1685.
24. P. L. Gai, O. Stephan, K. McGuire, A. M. Rao, M. S. Dresselhaus, G. Dresselhaus and C. Colliex, *J. Mater. Chem.*, 2004, **14**, 669-675.
25. W. Q. Han, Y. Bando, K. Kurashima and T. Sato, *Chem. Phys. Lett.*, 1999, **299**, 368-373.
26. E. Borowiak-Palen, T. Pichler, G. G. Fuentes, A. Graff, R. J. Kalenczuk, M. Knupfer and J. Fink, *Chem. Phys. Lett.*, 2003, **378**, 516-520.
27. D. Golberg, Y. Bando, L. Bourgeois, K. Kurashima and T. Sato, *Carbon*, 2000, **38**, 2017-2027.
28. E. Borowiak-Palen, T. Pichler, A. Graff, R. J. Kalenczuk, M. Knupfer and J. Fink, *Carbon*, 2004, **42**, 1123-1126.
29. D. Golberg, Y. Bando, W. Han, K. Kurashima and T. Sato, *Chem. Phys. Lett.*, 1999, **308**, 337-342.

30. X. X. Yang, L. Liu, M. H. Wu, W. L. Wang, X. D. Bai and E. G. Wang, *J. Am. Chem. Soc.*, 2011, **133**, 13216-13219.
31. W.-H. Chiang, D. N. Futaba, M. Yumura and K. Hata, *Carbon*, 2011, **49**, 4368-4375.
32. S. Attal, R. Thiruvengadathan and O. Regev, *Anal. Chem.*, 2006, **78**, 8098-8104.
33. A. Lapicki, D. M. Peiris, J. N. Smolanoff and S. L. Anderson, *J. Phys. Chem. A*, 1999, **103**, 226-234.
34. W.-H. Chiang, D. N. Futaba, M. Yumura and K. Hata, *J. Nanosci. Nanotechnol.*, 2013, **13**, 2745-2751.
35. X. M. Liu, H. E. Romero, H. R. Gutierrez, K. Adu and P. C. Eklund, *Nano Lett.*, 2008, **8**, 2613-2619.
36. S. Suzuki, M. Tomita and T. Hayashi, *Jpn. J. Appl. Phys. 2*, 1995, **34**, L191-L194.
37. L. L. Sun, T. Matsuoka, Y. Tamari, K. Shimizu, J. F. Tian, Y. A. Tian, C. D. Zhang, C. M. Shen, W. Yi, H. J. Gao, J. Q. Li, X. L. Dong and Z. X. Zhao, *Phys. Rev. B*, 2009, **79**, 140505(R).
38. R. J. Nicholls, Z. Aslam, M. C. Sarahan, A. Koos, J. R. Yates, P. D. Nellist and N. Grobert, *ACS Nano*, 2012, **6**, 7800-7805.
39. P. Ayala, J. Reppert, M. Grobosch, M. Knupfer, T. Pichler and A. M. Rao, *Appl. Phys. Lett.*, 2010, **96**, 183110.
40. D. P. Hashim, N. T. Narayanan, J. M. Romo-Herrera, D. A. Cullen, M. G. Hahm, P. Lezzi, J. R. Suttle, D. Kelkhoff, E. Munoz-Sandoval, S. Ganguli, A. K. Roy, D. J. Smith, R. Vajtai, B. G. Sumpter, V. Meunier, H. Terrones, M. Terrones and P. M. Ajayan, *Sci. Rep.*, 2012, **2**, 363.
41. J. Vetrone, J. Fan and M. Trenary, *Surf. Sci.*, 1994, **314**, 315-324.
42. S. Wu, X. Q. Lan, F. F. Huang, Z. Z. Luo, H. X. Ju, C. G. Meng and C. Y. Duan, *Biosens. Bioelectron.*, 2012, **32**, 293-296.
43. T. W. Lin, C. Y. Su, X. Q. Zhang, W. Zhang, Y. H. Lee, C. W. Chu, H. Y. Lin, M. T. Chang, F. R. Chen and L. J. Li, *Small*, 2012, **8**, 1384-1391.
44. X. Yu and H. S. Park, *Carbon*, 2014, **77**, 59-65.

45. M. S. Dresselhaus, G. Dresselhaus, R. Saito and A. Jorio, *Phys. Rep.*, 2005, **409**, 47-99.
46. J. Maultzsch, S. Reich, C. Thomsen, S. Webster, R. Czerw, D. L. Carroll, S. M. C. Vieira, P. R. Birkett and C. A. Rego, *Appl. Phys. Lett.*, 2002, **81**, 2647-2649.
47. M. S. Dresselhaus and G. Dresselhaus, *Adv. Phys.*, 2002, **51**, 1-186.
48. S. D. M. Brown, A. Jorio, P. Corio, M. S. Dresselhaus, G. Dresselhaus, R. Saito and K. Kneipp, *Phys. Rev. B*, 2001, **63**, 155414.
49. D. N. Futaba, T. Yamada, K. Kobashi, M. Yumura and K. Hata, *J. Am. Chem. Soc.*, 2011, **133**, 5716-5719.
50. M. Sankaran and B. Viswanathan, *Carbon*, 2007, **45**, 1628-1635.
51. T. Shirasaki, A. Derre, M. Menetrier, A. Tressaud and S. Flandrois, *Carbon*, 2000, **38**, 1461-1467.
52. B. Ottaviani, A. Derre, E. Grivei, O. A. M. Mahmoud, M. F. Guimon, S. Flandrois and P. Delhaes, *J. Mater. Chem.*, 1998, **8**, 197-203.
53. Y. A. Kim, K. Fujisawa, H. Muramatsu, T. Hayashi, M. Endo, T. Fujimori, K. Kaneko, M. Terrones, J. Behrends, A. Eckmann, C. Casiraghi, K. S. Novoselov, R. Saito and M. S. Dresselhaus, *ACS Nano*, 2012, **6**, 6293-6300.
54. D. L. Carroll, P. Redlich, X. Blase, J. C. Charlier, S. Curran, P. M. Ajayan, S. Roth and M. Rühle, *Phys. Rev. Lett.*, 1998, **81**, 2332-2335.
55. W. Shen, H. Li, C. Wang, Z. H. Li, Q. J. Xu, H. M. Liu and Y. G. Wang, *J. Mater. Chem. A*, 2015, **3**, 15190-15201.
56. C. Wang, Z. Y. Guo, W. Shen, Q. J. Xu, H. M. Liu and Y. G. Wang, *Adv. Func. Mater.*, 2014, **24**, 5511-5521.

Figure captions

Figure 1 Schematic illustration of stepwise, postgrowth substitution reaction route to produce BCNTs. The stepwise reaction route is composed with a wet-chemistry-assisted pretreatment and an atmospheric pressure carbothermic reaction.

Figure 2 Representative (a) SEM, (b) TEM, and (c) HRTEM images of the starting MWCNTs synthesized by a catalytic CVD. (d) SEM, (e) TEM, and (f) HRTEM images of the as-produced BCNTs prepared at 1200 °C for 4 h (sample B3 in Table S1) by the developed postgrowth substitution reaction.

Figure 3 (a) Representative EELS spectrum and (b) enlarged B K-edge EELS spectrum of the as-produced BCNTs. (c) HAADF-STEM image of the as-produced BCNTs. The EELS mapping of (d) B and (e) C of the as-produced BCNTs. The as-produced BCNTs were prepared at 1200 °C for 4 h (sample B3 in Table S1) by the developed postgrowth substitution reaction.

Figure 4 (a) The XPS survey spectra for the starting MWCNTs and the as-produced BCNTs prepared by the developed postgrowth substitution reaction. The peaks assigned to B1s, C1s, and O1s are indicated. (b) The enlarged plot for B1s peaks for starting MWCNTs and the as-produced BCNTs. (c) The plot of B dopant concentration as a function of reaction temperature. The as-produced BCNTs prepared from starting materials without the wet-chemistry-assisted pretreatment (sample A1-A3 in Table S1) were shown as the comparison.

Figure 5 HRXPS spectra of C1s region of as-produced BCNTs of (a) A3, (b) B3, and (c) B6. HRXPS spectra of B1s region of as-produced BCNTs of (d) A3, (e) B3, and (f) B6. (g) Schematic

structure of the bonding configuration of B doping in a carbon lattice. B1, B2, B3, and B4 denote the B_4C , BC_3 , BC_2O , and BCO_2 bonding configuration. The as-produced BCNTs were prepared by the developed postgrowth substitution reaction (Table S1).

Figure 6 (a) Raman spectra of pristine CNTs and as-produced BCNTs. (b) The I_D/I_G versus the B dopant concentrations in the as-synthesized BCNTs. (c) Enlarged G-band feature for pristine CNTs and as-produced BCNTs. G^+ and G^- are indicated. (d) The corresponding G^+ frequency (ω_{G^+}) and G^- frequency (ω_{G^-}) frequency of the as-produced BCNTs. The G-band frequency of pristine CNTs is indicated.

Figure 7 (a) XRD pattern of pristine CNTs and as-produced BCNTs. (b) The plot of $\Delta 2\theta$, the (002) Bragg peaks position difference between the as-produced BCNTs and pristine CNTs, as the function of the B concentration in the as-produced BCNTs. Linear fitting is shown for comparison. (c) The plot of calculated interlayer spacing of (002) plane of the as-produced BCNTs as the B concentration in the as-produced BCNTs. Linear fitting is shown for comparison.

Figure 8 (a) The averaged sheet resistances of the films of pristine CNTs and the as-synthesized BCNTs. The inset shows the enlarged plot of the averaged sheet resistances of the films of the as-synthesized BCNTs. The error bars are shown to indicate the standard deviation. (b) The distributions of B-C-O bonding configurations including BC_3 , BC_2O , and BCO_2 in the as-produced BCNTs from the HRXPS result (Fig. 5 and Fig. S2)

Figures

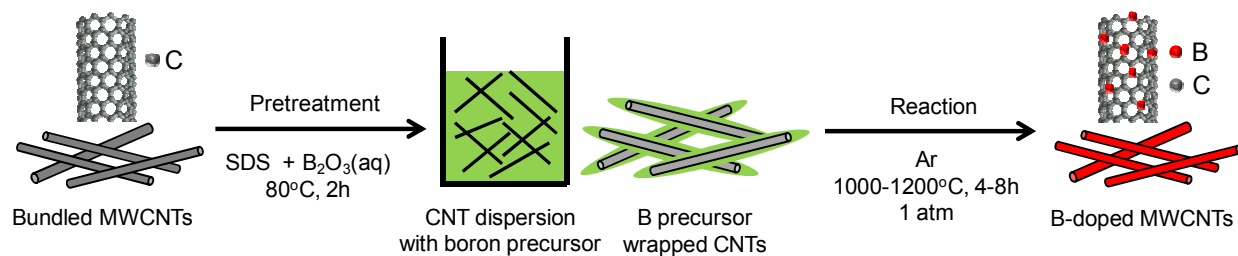


Figure 1 Schematic illustration of stepwise, postgrowth substitution reaction route to produce BCNTs. The stepwise reaction route is composed with a wet-chemistry-assisted pretreatment and an atmospheric pressure carbothermic reaction.

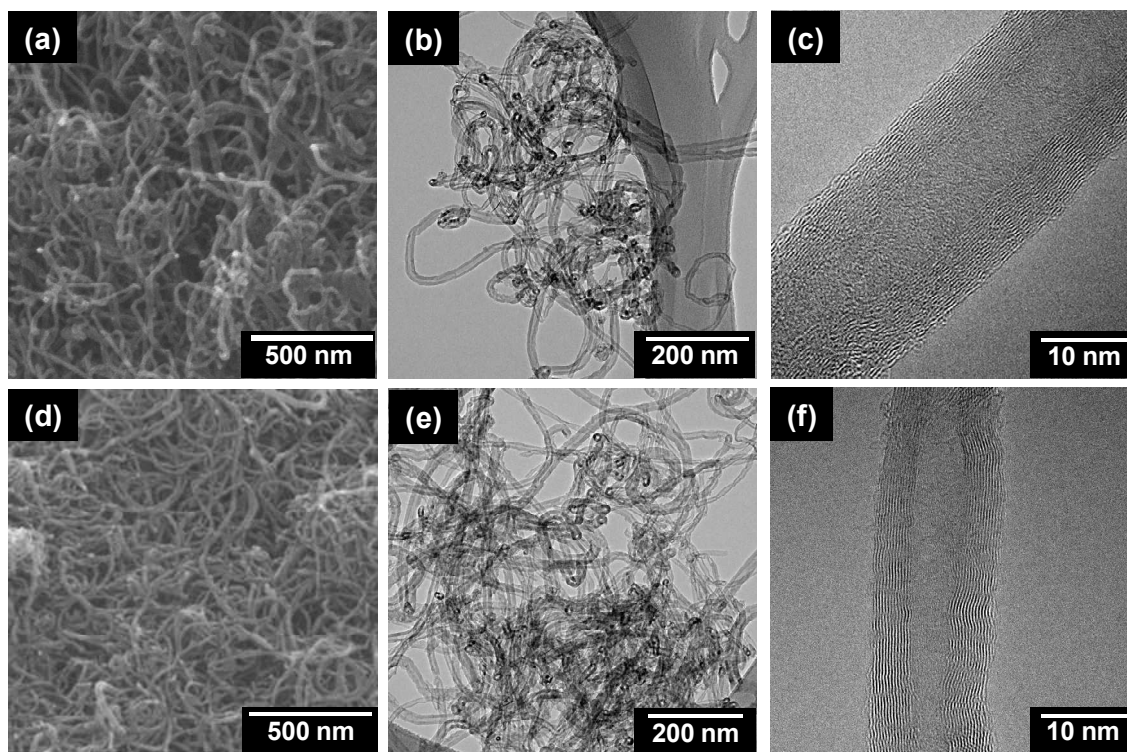


Figure 2 (a) SEM, (b) TEM, and (c) HRTEM images of the starting MWCNTs synthesized by a catalytic CVD. (d) SEM, (e) TEM, and (f) HRTEM images of the as-produced BCNTs prepared at 1200 °C for 4 h (sample B3 in Table S1) by the developed postgrowth substitution reaction.

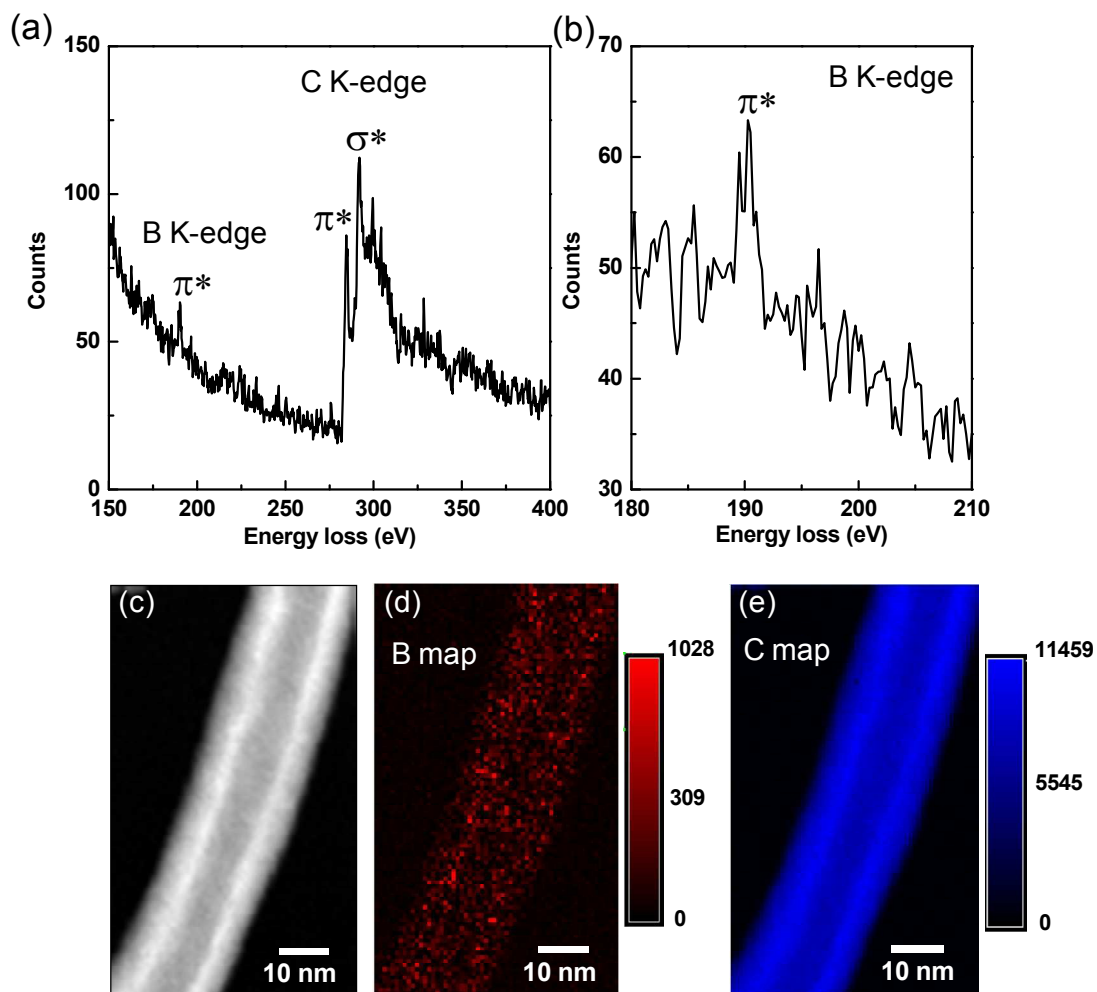


Figure 3 (a) Representative EELS spectrum and (b) enlarged B K-edge EELS spectrum of the as-produced BCNTs. (c) HAADF-STEM image of the as-produced BCNTs. The EELS mapping of (d) B and (e) C of the as-produced BCNTs. The as-produced BCNTs were prepared at 1200 °C for 4 h (sample B3 in Table S1) by the developed postgrowth substitution reaction.

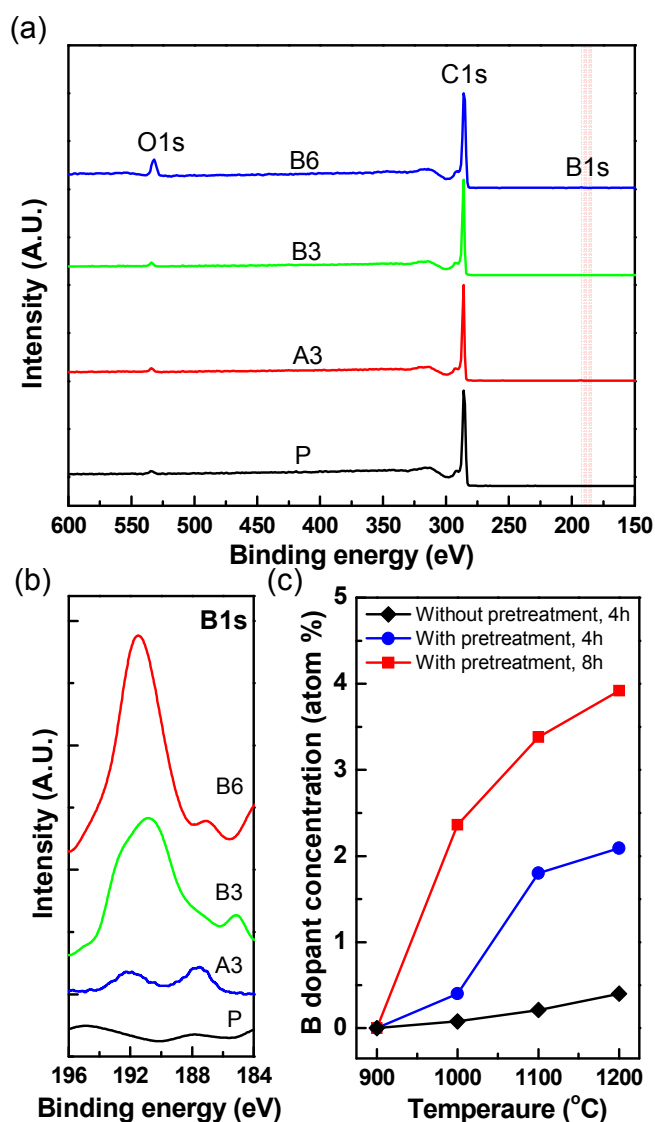


Figure 4 (a) The XPS survey spectra for the starting MWCNTs and the as-produced BCNTs prepared by the developed postgrowth substitution reaction. The peaks assigned to B1s, C1s, and O1s are indicated. (b) The enlarged plot for B1s peaks for starting MWCNTs and the as-produced BCNTs. (c) The plot of B dopant concentration as a function of reaction temperature. The as-produced BCNTs prepared from starting materials without the wet-chemistry-assisted pretreatment (sample A1-A3 in Table S1) were shown as the comparison.

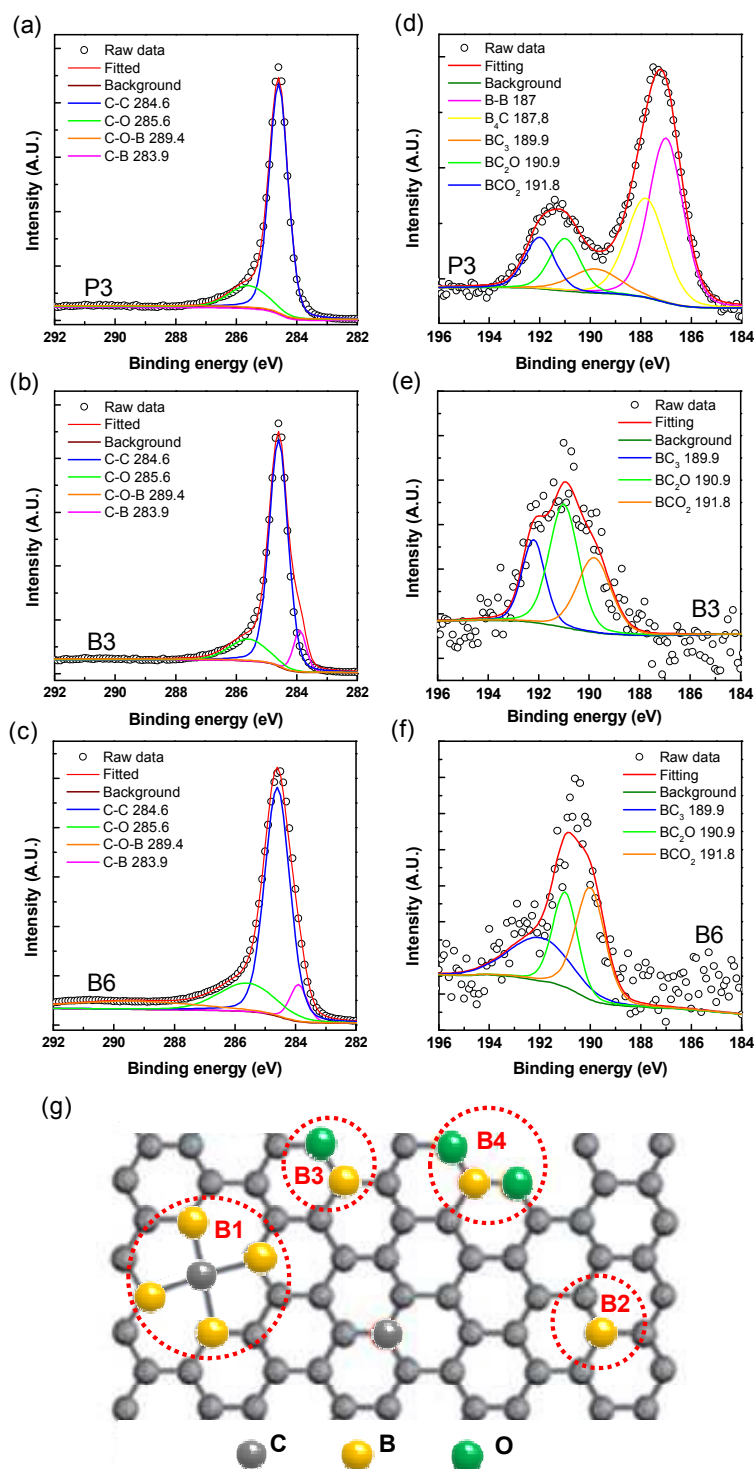


Figure 5 HRXPS spectra of C1s region of as-produced BCNTs of (a) A3, (b) B3, and (c) B6. HRXPS spectra of B1s region of as-produced BCNTs of (d) A3, (e) B3, and (f) B6. (g) Schematic

structure of the bonding configuration of B doping in a carbon lattice. B1, B2, B3, and B4 denote the B_4C , BC_3 , BC_2O , and BCO_2 bonding configuration. The as-produced BCNTs were prepared by the developed postgrowth substitution reaction (Table S1).

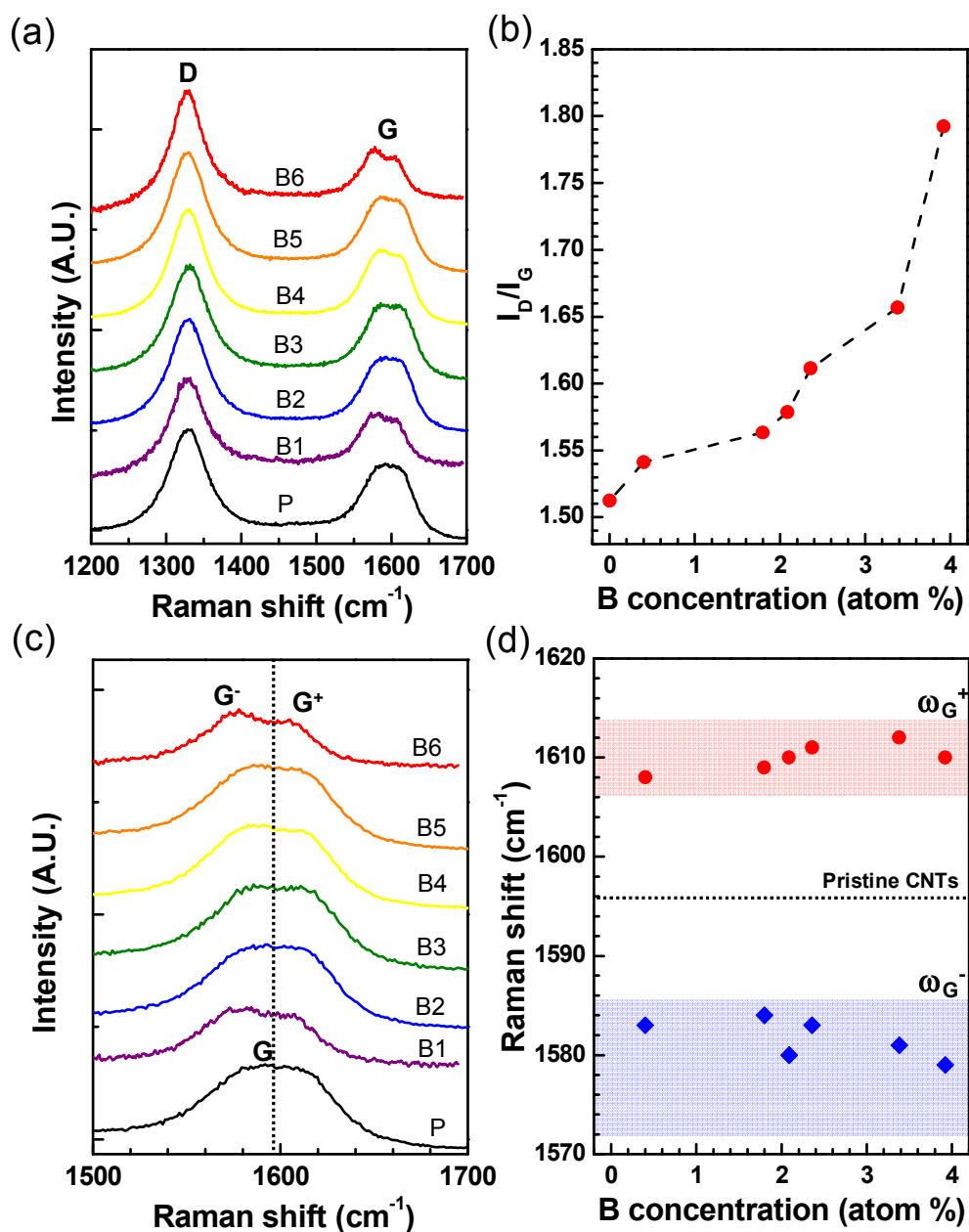


Figure 6 (a) Raman spectra of pristine CNTs and as-produced BCNTs. (b) The I_D/I_G versus the B dopant concentrations in the as-synthesized BCNTs. (c) Enlarged G-band feature for pristine CNTs and as-produced BCNTs. G^+ and G^- are indicated. (d) The corresponding G^+ frequency (ω_{G^+}) and G^- frequency (ω_{G^-}) frequency of the as-produced BCNTs. The G-band frequency of pristine CNTs is indicated.

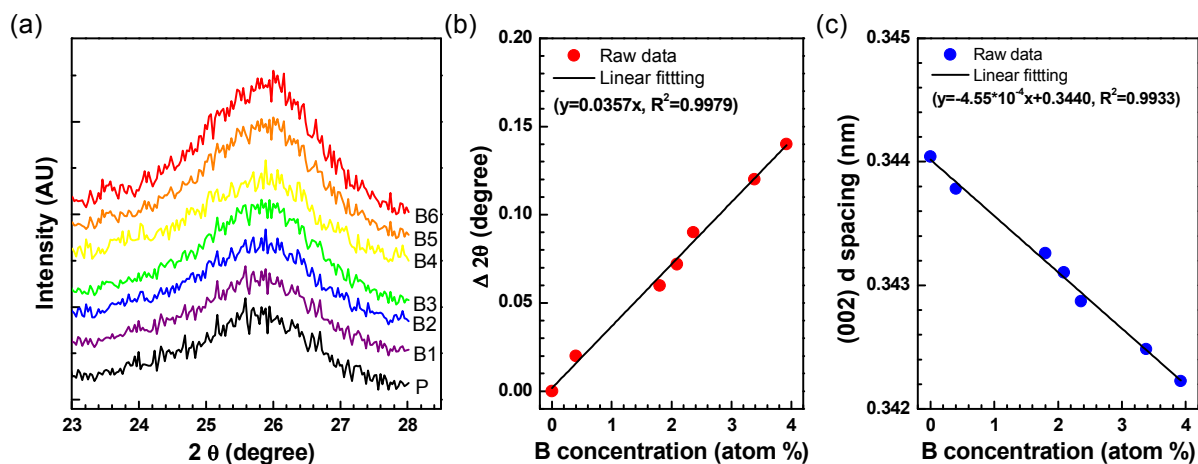


Figure 7 (a) XRD pattern of pristine CNTs and as-produced BCNTs. (b) The plot of $\Delta 2\theta$, the (002) Bragg peaks position difference between the as-produced BCNTs and pristine CNTs, as the function of the B concentration in the as-produced BCNTs. Linear fitting is shown for comparison. (c) The plot of calculated interlayer spacing of (002) plane of the as-produced BCNTs as the B concentration in the as-produced BCNTs. Linear fitting is shown for comparison.

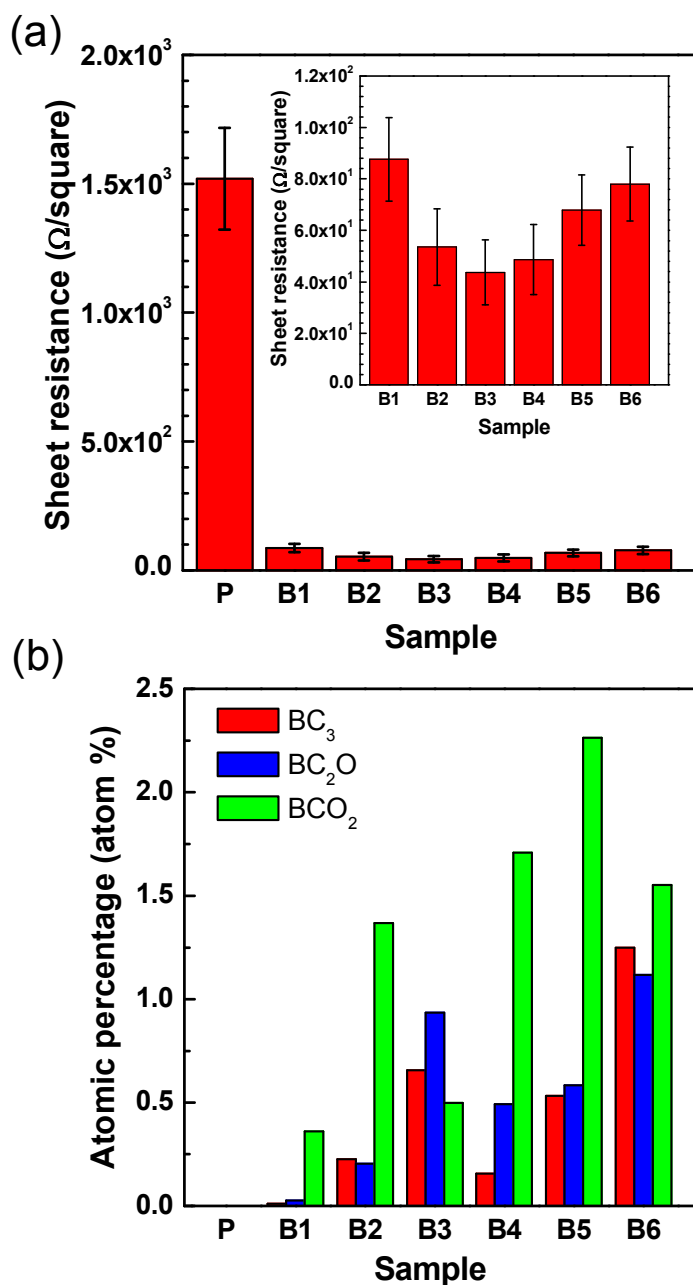


Figure 8 (a) The averaged sheet resistances of the films of pristine CNTs and the as-synthesized BCNTs. The inset shows the enlarged plot of the averaged sheet resistances of the films of the as-synthesized BCNTs. The error bars are shown to indicate the standard deviation. (b) The distributions of B-C-O bonding configurations including BC₃, BC₂O, and BCO₂ in the as-produced BCNTs from the HRXPS result (Fig. 5 and Fig. S3)